

A hybrid double-dot in silicon

This article has been downloaded from IOPscience. Please scroll down to see the full text article.

2012 New J. Phys. 14 023050

(<http://iopscience.iop.org/1367-2630/14/2/023050>)

View [the table of contents for this issue](#), or go to the [journal homepage](#) for more

Download details:

IP Address: 131.111.184.70

The article was downloaded on 24/10/2012 at 12:11

Please note that [terms and conditions apply](#).

A hybrid double-dot in silicon

M Fernando Gonzalez-Zalba¹, Dominik Heiss¹
and Andrew J Ferguson²

Microelectronics, Cavendish Laboratory, Cambridge University,
Cambridge, UK

E-mail: ajf1006@cam.ac.uk

New Journal of Physics **14** (2012) 023050 (11pp)

Received 15 November 2011

Published 21 February 2012

Online at <http://www.njp.org/>

doi:10.1088/1367-2630/14/2/023050

Abstract. We report electrical measurements of a single arsenic dopant atom in the tunnel barrier of a silicon single-electron transistor (SET). In addition to performing the electrical characterization of the individual dopant, we study the series electrical transport through the dopant and SET. We measure the triple points of this hybrid double-dot, using simulations to support our results, and show that we can tune the electrostatic coupling between the two sub-systems.

The study of single dopants in silicon is motivated by the prospect of quantum computation with long-lived electronic and nuclear spins [1]. The observation of individual dopant states in nanoscale field effect transistors was an important advance towards this goal. Electrical transport spectroscopy has enabled positive identification of dopants [2–4] as well as the investigation of their energy level structure in the presence of an interface [5, 6]. More recently, spin readout of a dopant electronic state was performed using a silicon single-electron transistor (SET) to sense the occupancy of a nearby dopant [7]. The ability to measure the dopant spin state is important for future experiments that probe the electron and nuclear spin coherence of single dopants.

A parallel direction in silicon-based quantum computation has been the development of few-electron quantum dots, where the spin state of single confined electrons (or electron pairs) is of interest. This follows the progress made in the GaAs material system, but with the advantage of a reduced nuclear spin environment. Specifically, in double quantum dots the well-established

¹ These authors contributed equally to this work.

² Author to whom any correspondence should be addressed.

mechanism of spin blockade enables the singlet and triplet states to be distinguished [8, 9]. In GaAs, this has enabled experiments on gate defined few-electron quantum dots, allowing the investigation of spin lifetime, spin coherence and exchange interaction between electrons in the two dots [10, 11]. In silicon, spin blockade has been observed in double quantum dots [12–14], and spin measurements carried out in single quantum dots [15–17].

In this paper, we report the electrical characterization of a double-dot formed from a single arsenic atom and a silicon SET. This approach combines the research on dopants and quantum dots and could provide a new way to read out the long-lived spin state of a dopant using spin blockade. In contrast to an earlier study [18], our SET is gate defined, allowing electrostatic control over both the dopant and SET and consequent observation and analysis of the triple points.

The device fabrication starts with the growth of a 10 nm sacrificial oxide on a high-resistivity ($>7000 \Omega \text{ cm}$) (100) silicon wafer. Ohmic contacts are defined by optical lithography and ion implantation of phosphorus (15 keV, 10^{15} cm^{-2}) and dopants included by low-dose (15 keV, 10^{11} cm^{-2}) ion implantation of arsenic. The sacrificial silicon oxide is removed after the implant, and a 10 nm SiO_2 gate oxide is regrown at 850°C , which also anneals out the implantation damage. We perform a forming gas anneal at 45°C for 30 min, followed by a rapid thermal anneal for 15 s at 1050°C to reduce the interface trap and fixed oxide charge density. The As profile was calculated by an implantation Monte-Carlo simulator³ and has a maximum at 10 nm from the interface and a density of $4 \times 10^{16} \text{ cm}^{-3}$. By comparison, the residual phosphorus doping is estimated to be smaller than 10^{12} cm^{-2} . We note that a larger As density at the interface is expected due to segregation to the interface during the thermal processing [19].

Subsequent to the silicon processing, surface gates are fabricated by electron beam lithography and thermal evaporation of aluminium. Figure 1 shows a scanning electron microscopy image of an identical device and its schematic cross-section. In a first step, two gates 40 nm wide and 100 nm apart are defined by evaporation of a 25 nm thick layer of aluminium. They are used to form the tuneable source and drain tunnel barriers. After thermal oxidation at 150°C for 5 min creating 5 nm aluminium oxide, a second electrically independent 60 nm thick top-gate is deposited over the barriers. This top-gate defines the 120 nm wide channel of the SET and leads that overlap with the doped ohmic contacts. Prior to measurement the samples undergo a nitrogen ambient post-fabrication anneal at 350°C for 15 min. The interface trap density, measured on simultaneously processed field effect transistors, by means of the low-frequency split C–V method [20], is $1.8 \times 10^{10} \text{ cm}^{-2}$.

The device can be operated in one of the three different modes depicted in figure 1: a SET (c), a single dopant (d) and a hybrid dopant–SET device (e). For SET operation, the top-gate is set well above threshold and the tunnel barriers are biased to locally deplete the electron accumulation layer underneath. This forms an isolated island of electrons between the barriers, leading to Coulomb oscillations in charge transport [21]. The second mode allows transport spectroscopy of individual As impurity atoms in the silicon substrate. The top-gate and drain tunnel barrier are biased well above threshold, allowing the study of subthreshold phenomena underneath the source tunnel barrier. Finally, the third mode of operation permits the formation of a tuneable capacitively coupled dopant–SET hybrid. Here, the SET is defined while one of the barriers is tuned in resonance with a dopant transition.

³ www.srim.org

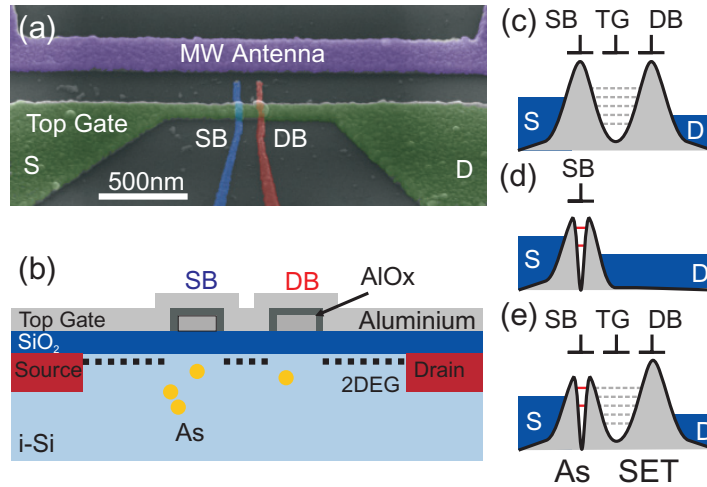


Figure 1. (a) Scanning electron microscopy image of an identical device. An on-chip coplanar stripline, for electron spin resonance, is included next to the sample but is not used in this experiment. (b) Schematic representation of the sample cross-section. (c–e) Schematic representation of the modes of device operation: (c) a SET, (d) a single dopant device and (e) a dopant–SET hybrid device.

Electrical transport measurements are made at the base temperature of a dilution refrigerator (electron temperature of 200 mK) using radio-frequency reflectometry [22]. This technique probes the reflection coefficient of a resonant circuit that includes the device as a circuit element. As the impedance, in our case the differential conductance, of the device changes, so does the reflection coefficient of the resonant circuit. This technique allows an increase of bandwidth over a standard dc or lock-in measurement. The sample was embedded in an rf-tank circuit formed by a surface mount 390 nH inductor and a parasitic capacitance (500 fF) to ground. An rf-carrier signal is applied to the source of the device at the resonant frequency of 360 MHz and the cryo-amplified reflected signal is homodyne detected [23]. A bias tee on the sample board permits the simultaneous measurement of the two-terminal dc conductance.

To form the SET tunnel barriers, a bias of 560 and 314 mV is applied to the source and drain barriers, respectively. Periodic Coulomb diamonds are observed over a large range of top-gate bias (figure 2), similar to earlier studies on undoped devices [21]. From the diamonds we extract a voltage period of $\Delta V_{\text{tg}} = 4.8$ mV and a charging energy of $E_c^{\text{SET}} = 1.4 \pm 0.1$ meV, which corresponds to $\alpha_{\text{SET}} = C_{\text{tg}}/C_{\text{SET}} = 0.29$, where C_{tg} is the capacitive coupling of the top-gate to the SET and C_{SET} is the total SET capacitance. Due to our gate geometry, where the top-gate controls electron density in the island as well as the leads, we are not able to deplete the SET to the few-electron limit. However, few-electron quantum dots have been measured in a similar geometry but with separated gates controlling the leads and the island [24–26].

We now describe electrical transport in the sub-threshold region beneath a single barrier, where we focus on the source barrier. The top-gate and drain barrier are set above threshold ($V_{\text{tg}} = 1.94$ V), while the rf response is measured as a function of V_{bs} (figure 3(a)) Below the conduction band edge ($V_{\text{bs}} = 430$ mV), the data show electrical transport through states labelled

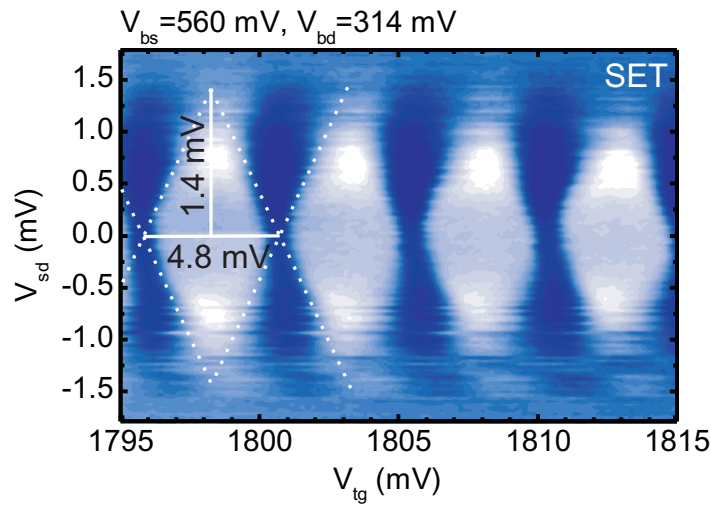


Figure 2. Measurement of the device in SET operation mode using rf reflectometry. Coulomb diamonds with a gate period of 4.8 mV and a charging energy of 1.4 meV are observed.

1, 2, and 3 in figure 3. These features appear at the same bias voltages in several cool-down cycles. We identify these states as dopants in the barrier due to their charging energies, as extracted from figures 3(c) and (d), being larger than 10 meV. In contrast, when we measure undoped samples, parasitic quantum dots are formed in the channel due to disorder at the interface, and these have a charging energy below 10 meV [27]. Transition 4 in figure 3 could arise from the formation of such a parasitic quantum dot, since the conductivity of this state is considerably larger and is found to be less than 10 meV below the conduction band edge. To further investigate the nature of states 1–3, we measured the line shape of the tunnel current as a function of temperature (symbols in figure 3(b)). This is fitted to the expected behaviour for resonant tunnelling through a discrete state (lines in figure 3(b)). In particular, the maximum current increases with decreasing temperature, in contrast to Coulomb blockade through a multi-level system such as the SET. This is consistent with transport through a dopant with well-separated energy levels ($\Delta E > k_B T$). Therefore, we attribute the transitions labelled 1, 2 and 3 to arsenic dopants, which typically show charging energies of the order of 29–35 meV close to the Si/SiO₂ interface [2, 5].

We next examine the coupling, given by $\alpha = C_{bs}/C_\Sigma$, of the barrier gate to the different dopant transitions. This coupling is a direct translation of V_{bs} to energy change on the dopant site. The obtained values were $\alpha_1 = 0.21$, $\alpha_2 = 0.10$ and $\alpha_3 = 0.08$. We expect the electrostatic characteristics of the device to change when changing the biasing conditions from $V_{bs} = 430$ mV to -630 mV. The capacitive coupling of a dopant to the gate electrode (C_{bs}) and the contacts (C_s, C_d) is inherently changed due to screening effects and changes in the effective barrier width as a function of V_{bs} . As a result, it is not possible to identify which transitions stem from the same dopant site by comparing these values alone.

We perform magneto-spectroscopy on these states, applying an in-plane magnetic field perpendicular to the current direction (figures 3(e)–(g)). The peak position is converted into a chemical potential shift using α and is in agreement with the expected Zeeman shift of $58 \mu\text{eV T}^{-1}$ for an electron with g -factor = 2. Transitions 1 and 3 shift to lower energies

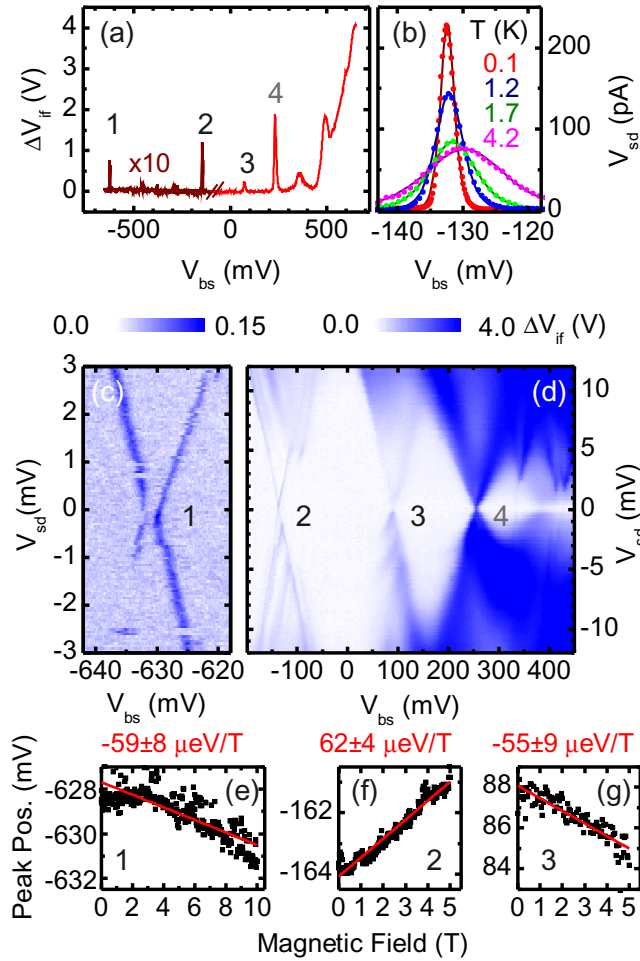


Figure 3. (a) Turn-off characteristics of the source tunnelling barrier. Subthreshold features labelled 1–4 are observed. (b) Tunnelling current of transition 2 as a function of temperature. In this measurement $V_{sd} = -0.1$ mV. (c, d) Coulomb diamonds of the subthreshold features. (e–g) Magnetic field dependence of the peak position of transitions 1, 2 and 3, respectively.

corresponding to transport through the lower Zeeman sub-level. This behaviour is expected for tunnelling through an ionized donor ($D^+ - D^0$ transition) [2, 5]. In contrast, transition 2 shifts to higher energies, suggesting that the lower Zeeman level is already occupied and tunnelling takes place through an already occupied (neutral) donor ($D^0 - D^-$ transition). Accordingly, we identify the three sub-threshold peaks as follows: 1 corresponds to the $D^+ - D^0$ transition of an As donor; 2 to the corresponding $D^0 - D^-$ transition; and 3 is identified as the $D^+ - D^0$ transition of an additional As donor. For typical donor charging energies of 29–35 meV we expect the corresponding $D^0 - D^-$ transition to be around $V_{bs} = 400$ mV, where several conductance peaks are observed that cannot be clearly identified.

Following this, the charging energy for transitions 1 and 2 is determined as $E_c = 73$ meV. Here, we use an average value of $\alpha_{1,2} = 0.155$ and bias voltage difference $\Delta V_{bs} = 470$ mV. Such an increased charging energy has not been observed so far, but may be a consequence of our relatively large dopant density, the presence of another ionized As atom leading to an increased

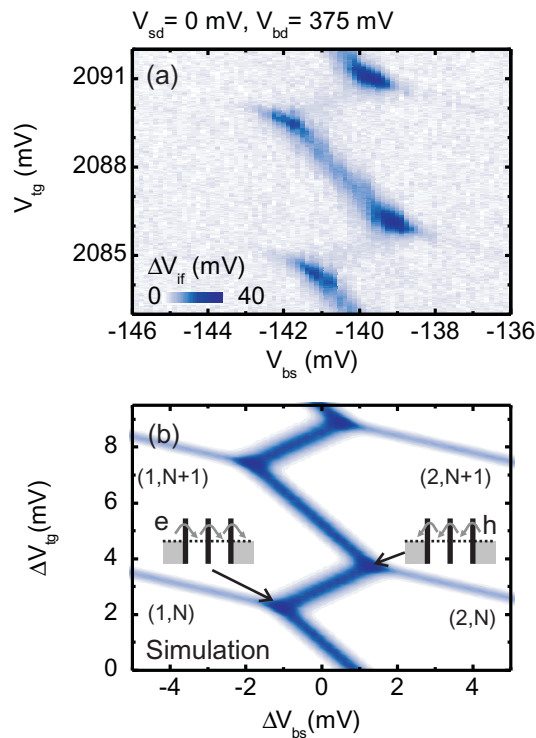


Figure 4. (a) Rf-reflectometry measurement as a function of top-gate bias V_{tg} and source barrier bias V_{bs} . Four triple points can be observed within this range. (b) Simulation of the measurement presented in (a). The charge state is labelled in the form (n, m) , where n denotes the number of electrons on the dopant site, while m stands for the electron number on the SET. The inset illustrates the difference between electron and hole transport processes.

ionization energy [28, 29]. Another possibility is that an orbital Stark shift [30] increases the observed charging energy. The electric field at the dopant site varies for the two transitions, due to the difference in biasing conditions. Additionally, a weaker screening effect induced by the metallic dominated interface is expected for the charged impurity atom in comparison to the neutral dopant [31].

Investigation of the drain barrier revealed two additional resonant tunnelling features consistent with transport through a neutral donor. As in the case of transition 3, the corresponding D^0 - D^- transition could not be clearly identified. Consequently, these states were not investigated further.

We now turn our attention to the hybrid dopant-SET system, investigating the sequential transport through a single dopant and the SET. A positive voltage of $V_{tg} = 2$ V is applied to the top-gate, while the drain barrier voltage is set to $V_{bd} = 375$ mV. The source barrier is tuned such that transport is governed by tunnelling through transition 2, since in this configuration the strongest dopant-SET coupling is observed.

Again using rf reflectometry, we measured the hybrid system formed by transition 2 and the SET, as a function of the top-gate voltage V_{tg} and barrier V_{bs} (figure 4(a)). As in a double quantum dot, electrical conduction occurs at points with threefold degeneracy of

the charge state, known as triple points [32]. Transport through the system can be described by a capacitance model, and we simulated the differential conductance to compare to the rf-reflectometry measurement (figure 4(b)). The software SIMON⁴ was used to calculate tunnelling probabilities by Monte-Carlo simulation. The SET was described as a metallic island with a constant density of states. The dopant was simulated as a discrete energy level system represented by delta functions. An excitation voltage of 125 μ V, corresponding to -97 dBm of rf power at the tank circuit, was used to obtain the differential conductance.

For increasing the top-gate voltage we observe the charge transitions of the SET with a gate period of $\Delta V_{\text{tg}} = 4.8$ mV, in agreement with the characterization of the SET alone (figure 4(b)). The dopant transition has been identified as D^0-D^- ; therefore, the electron number increases from 1 to 2 for increasing barrier voltage V_{bs} . Weak lines of increased conductance are observable at the charge transitions due to elastic co-tunnelling processes [33, 34].

In the finite bias regime $|V_{\text{sd}}| > 0$ the conductance regions change from triple points to triangles (figure 5(a)). We measure (figures 5(b) and (c)) and simulate (figures 5(d) and (e)) these bias triangles for both bias polarities. The dimensions of the bias triangles are related to the bias voltage through the corresponding values of α , $\alpha_{\text{bs}} = e|V_{\text{sd}}|/\delta V_{\text{bs}}$ and $\alpha_{\text{tg}} = e|V_{\text{sd}}|/\delta V_{\text{tg}}$. From the measurement presented in figures 5(b) and (c), we can extract $\alpha_{\text{bs}} = 0.16$ and $\alpha_{\text{tg}} = 0.28$ for the dopant site and the SET, respectively. Despite the change in biasing, this is in reasonable agreement with the values obtained from isolated measurement of the dopant ($\alpha_2 = 0.10$) and the SET ($\alpha_{\text{SET}} = 0.29$) stability diagram.

An additional feature parallel to the dopant line is visible within the bias triangle (figure 5(b)), at an energy of 0.27 ± 0.03 meV from the ground state. Such lines of increased differential conductance within the bias triangle can arise from modulation of density of states in the leads [35]. Alternatively, such features can be observed when the energy level of an excited dopant state enters the bias window. We cannot distinguish the origin of this line, but note that in the $2e$ configuration of a dopant a valley-spin-excited state around 1 meV has been observed [36]. We do not detect the additional line for $V_{\text{sd}} = 0.8$ meV, which is a consequence of the asymmetry in the hybrid system.

We will now discuss the coupling of the dopant and the SET. A measure of the electrostatic coupling of the SET to the dopant is the ratio $C_{\text{m}}/C_{\text{SET}} = \Delta V_{\text{bs}}^{\text{m}}/\Delta V_{\text{bs}}$ [37], where C_{m} is the mutual capacitance between the SET and the dopant. The induced voltage change of the dopant line at the triple points $\Delta V_{\text{bs}}^{\text{m}}$ can be extracted from the measurement, as indicated in figure 6(d), and $\Delta V_{\text{bs}} = 470$ mV is the separation of the D^+-D^0 and the D^0-D^- transition of the dopant. The data in figure 4(a) show $\Delta V_{\text{bs}}^{\text{m}} = 2.3$ mV, resulting in $C_{\text{m}}/C_{\text{SET}} = 0.008$. In analogy, the electrostatic effect of the dopant on the SET is $C_{\text{m}}/C_{\text{As}} = \Delta V_{\text{tg}}^{\text{m}}/\Delta V_{\text{tg}} = 0.53$. Using the previously determined total capacitance of the dopant $C_{\text{As}} = 2.1$ aF and the SET $C_{\text{SET}} = 116$ aF a mutual capacity of $C_{\text{m}} = 1.0 \pm 0.2$ aF is estimated. Under these conditions the maximum source–drain current measured at the triple point for $V_{\text{sd}} = -0.65$ mV is 130 pA, which corresponds to a tunnelling time of 1.2 ns between the dopant and the SET.

Furthermore, the dopant–SET coupling can be tuned by changing the bias on the drain tunnel barrier V_{bd} (figure 6(a)–(c)). In figures 6(e) and (f), the electrostatic coupling $C_{\text{m}}/C_{\text{SET}}$ and $C_{\text{m}}/C_{\text{As}}$ is plotted as a function of V_{bd} . As the voltage on the drain tunnel barrier is increased, the separation of the triple points decreases, which corresponds to a reduced electrostatic coupling between the dopant and the SET. This change arises partly from a reduced capacitive

⁴ www.lybrary.com/simon/

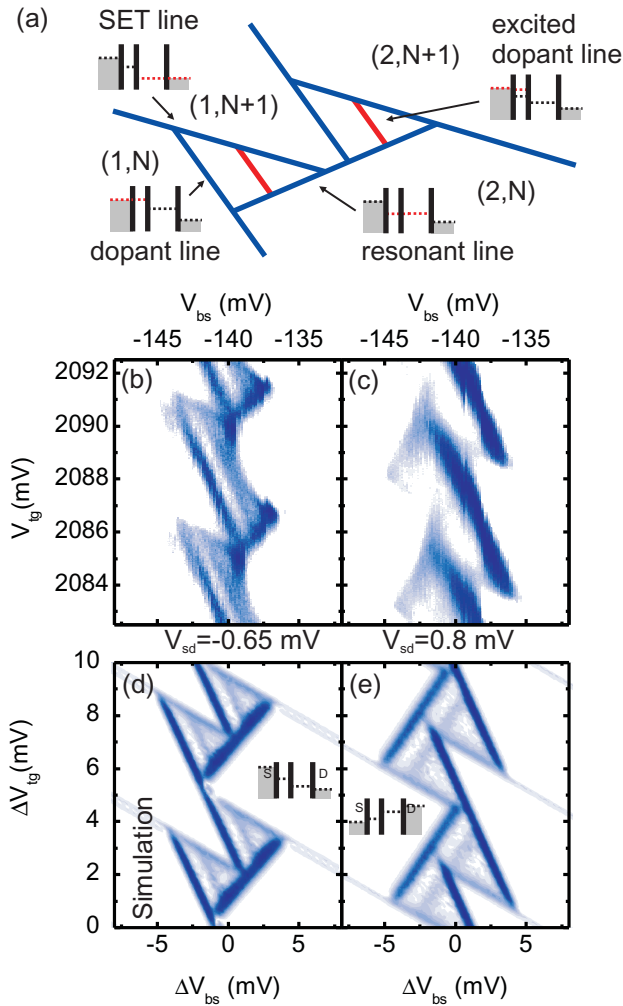


Figure 5. (a) Schematic representation of the bias triangles observed for $V_{sd} < 0$. The resonant conditions defining the borders of the triangles are indicated. (b, c) rf-reflectometry measurement of the hybrid system for $V_{sd} = -0.65$ and 0.8 mV, respectively. (d, e) Simulation of the measurement presented in (b, c). The SET is described by the capacitive coupling to drain $C_d = 74$ aF, the top-gate $C_{tg} = 34$ aF and a total capacitance $C_{SET} = 116$ aF. For the dopant we find the source ($C_s = 0.7$ aF), barrier ($C_{bs} = 0.34$ aF) and total ($C_{As} = 2.1$ aF) capacitance.

coupling C_m as the SET island extends further away from the dopant site, partly from an increased C_{SET} as the SET is coupled more strongly to the drain lead.

To conclude, we have studied a hybrid double dot formed by coupling a dopant and an SET in series. In transport spectroscopy, we observe triple points and bias triangles characteristic of a double quantum dot. The analogy with the double quantum dot could be taken further by reducing the SET to the few-electron limit. This can be achieved by reducing the geometrical size of the SET or adding an extra plunger gate to independently control the electron occupancy in the dot. In the few-electron regime, such an SET would exhibit well-defined spin quantum

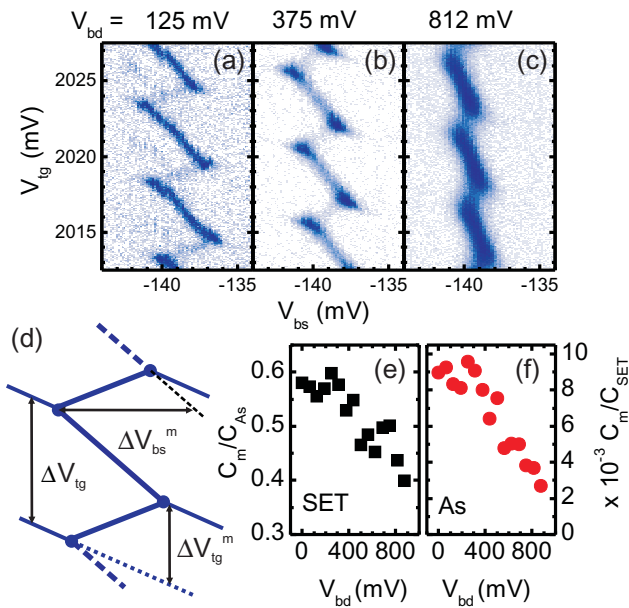


Figure 6. (a–c) The triple points of the hybrid system for drain barrier voltages $V_{bd} = 125, 375$ and 812 mV, respectively. (d) Schematic representation of the triple point measurement indicating the voltage separation ΔV_{bs}^m , ΔV_{tg} and ΔV_{tg}^m . (e, f) Electrostatic coupling C_m/C_{As} and C_m/C_{SET} as a function of drain barrier bias V_{bd} .

numbers. As a consequence, the hybrid system could be tuned into a configuration where transport is suppressed due to Pauli spin blockade. The magnetic field dependence of the leakage current in the spin blockade regime can reveal spin dynamics, as demonstrated with double quantum dots on GaAs [38] and silicon [39]. Furthermore, spin resonance experiments allow the investigation of spin coherence properties [40]. Here, the spin-blockade can be lifted with the application of microwave pulses via an on-chip waveguide, which results in an increased conductivity in resonance condition. This will provide a new device architecture for the investigation of the spin dynamics and coherence properties of electron spins on the dopant or the quantum dot.

Acknowledgments

We acknowledge support from EPSRC grant no. EP/H016872/1 and the Hitachi Cambridge Laboratory. AJF was supported by a Hitachi Research Fellowship. We acknowledge discussions with David Williams. MFGZ was supported by an Obra Social La Caixa fellowship.

References

- [1] Kane B E 1998 A silicon-based nuclear spin quantum computer *Nature* **393** 133–7
- [2] Sellier H, Lansbergen G P, Caro J, Rogge S, Collaert N, Ferain I, Jurczak M and Biesemans S 2006 Transport spectroscopy of a single dopant in a gated silicon nanowire *Phys. Rev. Lett.* **97** 206805

- [3] Ono Y, Nishiguchi K, Fujiwara A, Yamaguchi H, Inokawa H and Takahashi Y 2007 Conductance modulation by individual acceptors in Si nanoscale field-effect transistors *Appl. Phys. Lett.* **90** 102106
- [4] Tan K Y *et al* 2010 Transport spectroscopy of single phosphorus donors in a silicon nanoscale transistor *Nano Lett.* **10** 11–5
- [5] Lansbergen G P, Rahman R, Wellard C J, Woo I, Caro J, Collaert N, Biesemans S, Klimeck G, Hollenberg L C L and Rogge S 2008 Gate-induced quantum-confinement transition of a single dopant atom in a silicon finFET *Nature Phys.* **4** 656–61
- [6] Pierre M, Wacquez R, Jehl X, Sanquer M, Vinet M and Cueto O 2010 Single-donor ionization energies in a nanoscale CMOS channel *Nature Nanotechnol.* **5** 133–7
- [7] Andrea Morello *et al* 2010 Single-shot readout of an electron spin in silicon *Nature* **467** 687–91
- [8] Ono K, Austing D G, Tokura Y and Tarucha S 2002 Current rectification by Pauli exclusion in a weakly coupled double quantum dot system *Science* **297** 1313–7
- [9] Johnson A C, Petta J R, Marcus C M, Hanson M P and Gossard A C 2005 Singlet-triplet spin blockade and charge sensing in a few-electron double quantum dot *Phys. Rev. B* **72** 165308
- [10] Hanson R, Kouwenhoven L P, Petta J R, Tarucha S and Vandersypen L M K 2007 Spins in few-electron quantum dots *Rev. Mod. Phys.* **79** 1217–65
- [11] Petta J R, Johnson A C, Taylor J M, Laird E A, Yacoby A, Lukin M D, Marcus C M, Hanson M P and Gossard A C 2005 Coherent manipulation of coupled electron spins in semiconductor quantum dots *Science* **309** 2180–4
- [12] Nakul Shaji *et al* 2008 Spin blockade and lifetime-enhanced transport in a few-electron Si/SiGe double quantum dot *Nature Phys.* **4** 540–4
- [13] Liu H W, Fujisawa T, Ono Y, Inokawa H, Fujiwara A, Takashina K and Hirayama Y 2008 Pauli-spin-blockade transport through a silicon double quantum dot *Phys. Rev. B* **77** 073310
- [14] Borselli M G *et al* 2011 Pauli spin blockade in undoped Si/SiGe two-electron double quantum dots *Appl. Phys. Lett.* **99** 063109
- [15] Xiao M, House M G and Jiang H W 2010 Measurement of the spin relaxation time of single electrons in a silicon metal-oxide-semiconductor-based quantum dot *Phys. Rev. Lett.* **104** 096801
- [16] Robert Hayes R *et al* 2009 Lifetime measurements (T_1) of electron spins in Si/SiGe quantum dots arXiv:0908.0173
- [17] Simmons C B *et al* 2011 Tunable spin loading and T_1 of a silicon spin qubit measured by single-shot readout *Phys. Rev. Lett.* **106** 156804
- [18] Golovach V N, Jehl X, Houzet M, Pierre M, Roche B, Sanquer M and Glazman L I 2011 Single-dopant resonance in a single-electron transistor *Phys. Rev. B* **83** 075401
- [19] Grove A S, Leistiko J O and Sah C T 1964 Redistribution of acceptor and donor impurities during thermal oxidation of silicon *J. Appl. Phys.* **35** 2695–701
- [20] Kommen J 1973 Investigation of most channel conductance in weak inversion *Solid State Electron.* **16** 801–10
- [21] Angus S J, Ferguson A J, Dzurak A S and Clark R G 2007 Gate-defined quantum dots in intrinsic silicon *Nano Lett.* **7** 2051–5
- [22] Schoelkopf R J, Wahlgren P, Kozhevnikov A A, Delsing P and Prober D E 1998 The radio-frequency single-electron transistor (rf-set): a fast and ultrasensitive electrometer *Science* **280** 1238–42
- [23] Angus S J, Ferguson A J, Dzurak A S and Clark R G A 2008 Silicon radio-frequency single electron transistor *Appl. Phys. Lett.* **92** 112103
- [24] Lim W H, Zwanenburg F A, Huebl H, Möttönen M, Chan K W, Morello A and Dzurak A S 2009 Observation of the single-electron regime in a highly tunable silicon quantum dot *Appl. Phys. Lett.* **95** 242102
- [25] Xiao M, House M G and Jiang H W 2010 Parallel spin filling and energy spectroscopy in few-electron Si metal-on-semiconductor-based quantum dots *Appl. Phys. Lett.* **97** 032103
- [26] Lim W H, Yang C H, Zwanenburg F A and Dzurak A S 2011 Spin filling of valley orbit states in a silicon quantum dot *Nanotechnology* **22** 335704
- [27] Podd G J, Angus S J, Williams D A and Ferguson A J 2010 Charge sensing in intrinsic silicon quantum dots *Appl. Phys. Lett.* **96** 082104

- [28] Koiller B, Hu X D and Das Sarma S 2006 Electric-field driven donor-based charge qubits in semiconductors *Phys. Rev. B* **73** 045319
- [29] Rajib Rahman Muller R P, Levy J E, Carroll M S, Gerhard Klimeck, Greentree A D and Hollenberg L C L 2010 Coherent electron transport by adiabatic passage in an imperfect donor chain *Phys. Rev. B* **82** 155315
- [30] Rahman R, Lansbergen G P, Park S H, Verduijn J, Klimeck G, Rogge S and Hollenberg L C L 2009 Orbital stark effect and quantum confinement transition of donors in silicon *Phys. Rev. B* **80** 165314
- [31] Rahman R, Lansbergen G P, Verduijn J, Tettamanzi G C, Park S H, Collaert N, Biesemans S, Klimeck G, Hollenberg L C L and Rogge S 2011 Electric field reduced charging energies and two-electron bound excited states of single donors in silicon *Phys. Rev. B* **84** 115428
- [32] van der Wiel W G, De Franceschi S, Elzerman J M, Fujisawa T, Tarucha S and Kouwenhoven L P 2002 Electron transport through double quantum dots *Rev. Mod. Phys.* **75** 1–22
- [33] De Franceschi S, Sasaki S, Elzerman J M, van der Wiel W G, Tarucha S and Kouwenhoven L P 2001 Electron cotunneling in a semiconductor quantum dot *Phys. Rev. Lett.* **86** 878–81
- [34] Liu H W, Fujisawa T, Hayashi T and Hirayama Y 2005 Pauli spin blockade in cotunneling transport through a double quantum dot *Phys. Rev. B* **72** 161305
- [35] Martin Fuechsle, Mahapatra S, Zwanenburg F A, Mark Friesen, Eriksson M A and Simmons M Y 2010 Spectroscopy of few-electron single-crystal silicon quantum dots *Nature Nanotechnol.* **5** 502–5
- [36] Lansbergen R, Rahman G P, Verduijn J, Tettamanzi G C, Collaert N, Biesemans S, Klimeck G, Hollenberg L C L and Rogge S 2010 Lifetime enhanced transport in silicon due to spin and valley blockade arXiv:1008.1381
- [37] Gento Yamahata, Yoshishige Tsuchiya, Shunri Oda, Durrani Z A K and Hiroshi Mizuta 2008 Control of electrostatic coupling observed for silicon double quantum dot structures *Japan. J. Appl. Phys.* **47** 4820–6
- [38] Koppens F H L *et al* 2005 Control and detection of singlet-triplet mixing in a random nuclear field *Science* **309** 1346–50
- [39] Lai N S, Lim W H, Yang C H, Zwanenburg F A, Coish W A, Qassemi F, Morello A and Dzurak A S 2011 Pauli spin blockade in a highly tunable silicon double quantum dot *Sci. Rep.* **1** 110
- [40] Koppens F H L, Buizert C, Tielrooij K J, Vink I T, Nowack K C, Meunier T, Kouwenhoven L P and Vandersypen L M K 2006 Driven coherent oscillations of a single electron spin in a quantum dot *Nature* **442** 766–71